Nature Environment and Pollution Technology
An International Quarterly Scientific Journal

p-ISSN: 0972-6268
(Print copies up to 2016)
e-ISSN: 2395-3454

Vol. 23 | No. 4 | pp. 1995-2008 | 2024

Original Research Paper

https://doi.org/10.46488/NEPT.2024.v23i04.008

Open Access Journal

Optimization, Characterisation and Evaluation of Biochar Obtained from Biomass of Invasive Weed *Crotalaria burhia*

Loveena Gaur and Poonam Poonia†
Department of Zoology, Jai Narain Vyas University, Jodhpur, Rajasthan, India
†Corresponding author: Poonam Poonia; poonam.poonia@yahoo.com

Nat. Env. & Poll. Tech.
Website: www.neptjournal.com

Received: 16-01-2024
Revised: 13-03-2024
Accepted: 22-03-2024

Key Words:
Biochar
Invasive weed
Crotolaria burhia
Response surface methodology
Biomass

ABSTRACT

Invasive weed plants are unwanted and hazardous waste biomass; and have extraordinary potential to serve as raw materials for biochar production. To evaluate the potentiality of invasive weed for bioenergy production in the form of biochar, *Crotolaria burhia* was investigated. The response surface modeling and optimization of the biochar parameters were conducted using the experimental design expert 13.0. The optimum value of the desirability function was obtained at a pyrolysis temperature of 450°C and a particle size of 50-100 mm. The model represents a p-value less than 0.0500 and a high F value, which denotes its reliable and accurate prediction of experimental data. A strong correlation was observed between actual and predicted values for biochar composites fixed carbon, carbon, surface area, pore size, and pore volume. In the present study, *C. burhia* biochar production was carried out by slow pyrolysis at 450°C under vacuum conditions. Biochar was found to be alkaline, with a 33.23% yield. Proximate analysis of *C. burhia* revealed 3.35% moisture content, 8.48% volatile matter, 81.24% fixed carbon and 6.94% ash content. The elemental analysis shows major concentrations of carbon, hydrogen, and oxygen as 57.77%, 6.123%, and 27.60%, respectively. Low H/C and O/C molar ratios were quantified as 0.10% and 0.47%, respectively. It possesses a honeycomb structure having mesoporous surface porosity with a surface area of 155.19m²/g and the presence of a remarkable concentration of mineral elements calcium and potassium. Biochar rich in hydroxyl, carboxylic, and alkene functional groups enhances its applicability areas. These findings make *C. burhia* a potential feedstock for the production of good-quality biochar.

INTRODUCTION

Weed plant biomass can be used as a potential source for biochar production. High dry matter, low water, and nutrient requirement, presence of high cellulose content, and ubiquitous nature make weeds very attractive feedstock for biochar production (Priya et al. 2014, Premjet 2018). Thus, the conversion of invasive weed biomass into biochar can be very helpful in the efficient management of weed species and the production of energy-valuable by-products such as biochar (Feng et al. 2021).

Biochar is defined as a porous carbon-rich product obtained from the thermal degradation of biomass, such as wood, agricultural residues, manures, activated sludge, energy crops, etc. Pyrolysis is one of the most common thermochemical processes to convert dry biomass into by-products like biochar, bio-oil, and non-condensable gases (Kambo & Dutta 2015, Sik et al. 2016). In this process, thermal decomposition of organic material is carried out under a limited supply of oxygen and at relatively low temperatures (<700°C) (Lehmann & Joseph 2009). Biochar yield depends on the type and properties of feedstock and pyrolysis conditions such as temperature, heating rate, pressure, etc. (Song & Guo 2012, Roy & Dias 2017). On the basis of temperature, heating rate, and residence time, pyrolysis is mainly of two types, i.e., fast pyrolysis and slow pyrolysis. The type of pyrolysis is employed according to the requirement of by-product (Tripathi et al. 2016). Fast pyrolysis is carried out for high liquid yield, i.e., bio-oil, whereas slow pyrolysis produces solid char as the main product (Bridgwater 2003). High temperatures yield less biochar due to more volatile production, which in turn generates more gases and liquid (Cheah et al. 2016, Daful & Chandraratne 2020). Slow pyrolysis efficiently yields biochar of about 35.0% from dry biomass weight and is typically operated at the temperature range of 300-550°C, a slow heating rate of 0.1 C/s to 0.8 C/s and a longer residence time of 5-30 min or 25-35 hat atmospheric pressure (Roy & Dias 2017, Tomczyk et al. 2020).

Around 700 species of *C. burhia* are found throughout the tropical and subtropical regions of the world, and about 300 species have been reported in India (Wanjala & Majinda 1999, Lewis 2005). *C. burhia* is an undershrub fibrous plant

of the family Fabaceae. It is most commonly found weed in arid parts of India (Punjab, Rajasthan, and Gujarat), West Pakistan, and Afghanistan. It grows extensively on dunes all over the desert region. Its common name is 'Khimp,' and in Rajasthan, it is locally known as 'Shiniyo' (Kumar et al. 2008). In the present study, a weedy biomass *C. burhia* was used as feedstock to produce biochar through slow and vacuum pyrolysis at 450°C and further characterized and evaluated for determining its application. Under the optimal condition, derived biochar was characterized using proximate analysis, elemental analysis, Brunauer-Emmet-Teller method (BET), Scanning Electron Microscopy (SEM), X-ray Energy Dispersive Spectrometry (EDX), and Fourier Transform Infrared Spectroscopy (FTIR).

MATERIALS AND METHODS

Biomass Collection, Preparation and Biochar Production

C. burhia was collected from Kasti village of Baori tehsil located in Jodhpur, Rajasthan, India (Fig. 1). The biomass samples were washed with water to remove any contamination and sun-dried for 10 days in an open, clean area. Dry Biomass was chopped to attain a uniform size of 50-100mm. After this, the dried samples were packed, weighed, and further processed for vacuum pyrolysis at the Department of Renewable Energy Engineering, MPUAT, Udaipur, Rajasthan, India (Fig. 2).

A vacuum pyrolyzer is composed of various components such as a biomass cartridge, pyrolysis chamber, vacuum pump, electric heaters, insulation, condensers (shell and tube type), and vacuum pump. Initially, the chopped dry feedstock was filled into a biomass cartridge. This cartridge was then inserted into a pyrolysis chamber, which is connected to shell and tube-type condensers and a vacuum pump. To achieve the desired temperature for pyrolysis, electric coils are rolled over the pyrolysis chamber (Pawar & Panwar 2022). In vacuum pyrolyzer, biochar was produced at the temperature of 450°C with a residence time of 1 hour and a reduced pressure of 10-12kPa. A carbon-rich solid material, 'biochar,' was collected and weighed after a cooling session of about three hours. Gases and vapors produced during pyrolysis were removed from the pyrolysis chamber by the vacuum pump. Shell and tube-type condensers trapped the gases produced and converted them into liquid oil, i.e., bio-oil. The yield of the biochar has been calculated by using the following formula given by Sadaka et al. (2014)

$$\text{Biochar yield (\%)} = \frac{\text{weight of biochar (gms)}}{\textit{weight of biomas (gms)}} \times 100$$

Characterisation of Biomass and Biochar

For pH analysis, the biochar sample was crushed into powdered form, and the solution was prepared in deionized water in a ratio of 1:10 (biochar: deionized water). The prepared solution was shaken for about one hour and then allowed to stand for 30 min. The pH was measured in Systronics 1010 pH meter after calibrating using buffers of pH 7 and 10. The proximate analysis of raw material and biochar was carried out for moisture content, volatile content, fixed carbon content, and ash content utilizing ASTM 3173-87 method. Carbon,

Fig. 1: *C. burhia* plant in field.

Fig. 2: Dried biomass and biochar of *C. burhia*.

hydrogen, nitrogen, sulfur of feedstock, and biochar were determined by elemental analyzer vario MICRO Cube. The total surface area, pore volume, and pore size of the biochar sample were determined by the BET analyzer Micromeritics, ASAP, 2010. The biochar samples were subjected to high-resolution Field Emission scanning electron microscope (FE-SEM), JEOL JSM 7100F, to study the microstructures of biochar, and some localized elemental compositions such as C, O, Na, Mg, and K were analyzed by EDX. The thermo-gravimetric analysis of the feedstock was performed on a TG-DTG analyzer (Model: STA 7300, Hitachi, Germany) to find out the mass loss with an increase in carbonized temperature. The infrared spectrum of powdered biochar was recorded on 8 cm^{-1} resolution by Cary 630 FTIR spectrometer to identify the presence of the functional group.

Optimization of Biochar Preparation Conditions by Response Surface Methodology (RSM)

To obtain the best quality of *C. burhia* biochar, RSM, a multivariate statistical technique, was used to optimize the preparation parameters and their responses. One of the frequently used RSM techniques is the central composite design (CCD). CCD was used to optimize the preparation conditions using feedstock particle size and pyrolytic temperature as independent variables and fixed carbon, carbon, surface area, pore size, and pore volume as responses. In the present application of RSM, -1 denotes less than 50 mm particle size, 0 denotes 50 to 100 mm particle size, and +1 denotes more than 100 mm particle size. In this design total of 13 runs were found, compared, and tested on the surface response. The Design Expert 13.0 was employed for experimental design, tabulation, and data analysis. For the evaluation of RSM results, analysis of variance (ANOVA), coefficient of determination (R^2), three-dimensional plots, and contour plots were analyzed. The ANOVA finding gives p-value and model F values. To optimize the process variables, the R^2 value, coefficient of variation (CV %), adjusted R^2 value, and predicted R^2 values were analyzed.

RESULTS AND DISCUSSION

Yield and pH of Biochar

A high yield of *C. burhia* was found at 33.23%. This is attributed to the slow pyrolysis with vacuum conditions and lignocellulosic herbaceous weedy feedstock with the presence of high inorganic elements (Tomczyk et al. 2020, Carrier et al. 2012). Biochars are mostly alkaline. The pH of *C. burhia* biochar was observed as 10.0. Similar observations of pH have been confirmed by various researchers (Zama et al. 2017) (Table 1). pH of biochar increases with an increase in pyrolysis temperature due to the removal of acidic functional groups and accumulation of alkaline inorganic substances (Yuan et al. 2011, Zhang & Liy 2015). The application of biochar as a fuel or soil fertility or as an adsorbent of organic and inorganic contaminants depends upon the pH of biochar. An increase in pH from 2.0 to 5.0 has been reported for the increase in the adsorption capacity of the metallic cations (Chen et al. 2011). Alkaline pH has been reported for enhanced adsorption of organic contaminants of industrial wastewater (Parshetti et al. 2013) and to correct the acidity of agricultural soil by increasing pH (Daful et al. 2021).

Proximate and Elemental Analysis

The proximate analysis of biomass and biochar of *C. burhia*

Table 1: pH of various biochars.

Biomass	Pyrolysis temperature [°C]	Residence time [min]	pH	Reference
C. burhia	450	60	10	Present study
Green waste	450	60	10	Ronsse et al. 2013
Buckwheat husk	450	-	9.7	Zama et al. 2017

is shown in Table 2. An increase in pyrolytic temperature increases carbon and ash content, whereas it decreases the volatile content and moisture content of biochar (Zhao et al. 2017, Domingues et al. 2017).In the present study also, thermo-degradation of raw biomass into biochar results in an increase in fixed carbon and ash content by 325.56 % and 92.77%, respectively, and a decrease in moisture content and volatile content by 52.54% and 87.93%, respectively. At higher temperatures, further cracking of volatiles into low molecular weight products like liquids and gases occurs, resulting in low volatile content in biochar (Park et al. 2014, Usman et al. 2015).

The composition of carbon and hydrogen determines the quality and calorific value of biochar. The molar ratios of O/C, H/C, N/C, and S/C decrease with an increase in temperature (Usman et al. 2015, Domingues et al. 2017). Devolatilization of biomass during pyrolysis causes the removal of hydrogen and oxygen over carbon, resulting in carbon-rich biochar (Lehmann & Joseph 2009). In the present study, the carbon content observed is 57.77%, whereas hydrogen, nitrogen, and oxygen contents are 6.123%, 1.52%, and 27.60%, respectively (Table 2). The H/C ratio indicates the degree of aromaticity in biochar (Uchimiya et al. 2010). The O/C molar ratio represents the extent of carbonization and its stability in the environment (Rodriguez et al. 2020). The H/C and O/C ratio were found as 0.10 and 0.47, respectively. Biochar with O/C less than 0.2-0.6 shows moderate stability with a half-life between 100-1000 years (Spokas 2010). Biochar with an H/C ratio less than 0.7 indicates a high degree of aromaticity (i.e., greater fused aromatic ring) in comparison to an H/C ratio greater than 0.7 (IBI 2015). Decreased H/C and O/C ratios in pine needles biochars were reported to be correlated with higher aromaticity and lower polarity (Chen et al. 2008). Thus, obtained biochar possesses good quality properties with an enduring ability in soil for 100-1000 years and could be used for soil fertility enhancement and carbon sequestration.

BET Analysis

The surface area, pore volume, and pore size of *C. burhia* were observed as 155.19 $m^2.g^{-1}$, 0.0545 $cm^3.g^{-1}$, and 2.37 nm, respectively. Surface area increases with temperature due to thermal cracking and the elimination of pore-blocking materials, whereas pore volume increases due to the gradual degradation of lignin, cellulose, and organic matter, resulting in the creation of channels or tubular structures (Li et al. 2013, Rafiq et al. 2016, Zhao et al. 2017). The release of more volatiles at high temperatures causes an increase in the number of pores (Shaaban et al. 2014). Biochar's surface has been reported to vary from 3 $m^2.g^{-1}$ for rice husk to 500 $m^2.g^{-1}$ for wood (Kan et al. 2016). Surface area and pore volume play a crucial role in adsorption, water holding, and cation exchange capacity in the removal of pollutants from soil and water and soil restoration in agriculture (Weber & Quicker 2018).

SEM/EDX Analysis

SEM micrographs give a detailed description of the distribution and arrangement of pores present in the biochar (Fig. 3). The observed range of pore diameter of *C. burhia* (2.37nm) lies between 2 to 50 nm. Thus they possess mesoporous structures (Wang et al. 2022). Based on outward appearance, pores resemble honey-comb like structures and are observed as polygonal, uneven, and fibrous due to aggregation of mineral components over the surface. The formation of pores occurs due to de-volatilization during the pyrolysis process (Masto et al. 2013).

Table 2: The proximate and elemental analysis of biomass and biochar of *C. burhia*.

C. burhia	Biomass	Biochar
Proximate analysis		
Moisture content [%]	7.06	3.35
Volatile content [%]	70.26	8.48
Fixed carbon [%]	19.09	81.24
Ash content [%]	3.60	6.94
Elemental analysis		
Carbon	39.59	57.77
Nitrogen	2.25	1.52
Hydrogen	9.942	6.123
Sulfur	0.000	0.067
Oxygen	44.618	27.60
H/C	0.25	0.10
O/C	1.12	0.47
N/C	0.05	0.02
S/C	0.000	0.001

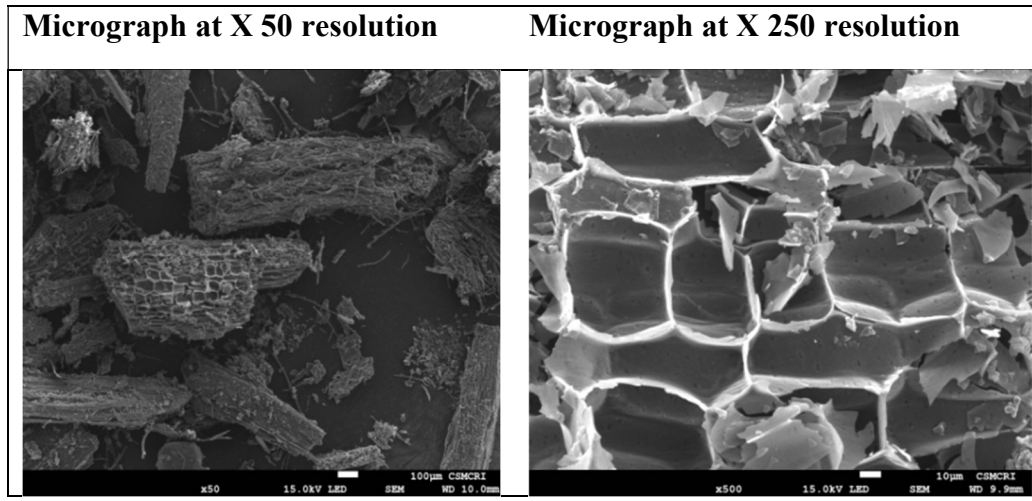

Fig. 3: SEM micrographs of *C. burhia* at different resolutions.

Biochars have profused mineral elements (Jha et al. 2010). Their concentration increases with an increase in temperature and varies with the type of biomass (de la Rosa et al. 2014). EDX indicated carbon (83.87%) and oxygen (13.78%) are major elements of the biochar. Some mineral elements in trace amount, such as Mg (0.35), Si (0.40), Cl (0.14), K (0.52), Ca (0.89), Br (0.05), were also detected (Table 3 and Fig. 4). Magnesium, potassium, and calcium are nutrient elements for plant growth (Qian et al. 2013, Rivka et al. 2017). A decrease in oxygen content indicates an increase in biochar surface hydrophobicity, which is an important factor in the removal of contaminants from an aqueous medium (Shaaban et al. 2014, Sik et al. 2016).

TG/DTG Analysis

Thermal gravimetry analysis (TGA) and differential thermal gravimetry (DTG) analysis provide a correlation between weight loss and temperature (Fig. 5). The TGA curve represents the thermal stability of biomass (Salavati-niasari et al. 2010). The thermal decomposition occurs in three zones. The first zone is the drying stage, in which thermal degradation occurs between 30°C - 150°C, with a mass loss of 8.33%. In this stage moisture content of biomass is removed by heating up to a temperature of 150°C (Yang et al. 2007). At a temperature of about <220°C devolatilisation of extractives of biomass takes place. The devolatilization stage is the second zone and is the most active stage of pyrolysis. The mass loss of about 83% occurred between temperatures of 150°C -400°C. In the de-volatilization stage, degradation of hemicellulose, cellulose, and lignin occurs. Hemicellulose degradation is observed at 150°C-270°C followed by degradation of cellulose at temperature range 270°C -400°C. Thermal degradation of lignin starts at 400°C and ends at 580°C, followed by carbonization. According to Yang et al. (2007), thermal degradation of hemicellulose and cellulose takes place in the temperature range of around 220°C-315°C and 315°C-400°C respectively, with maximum mass loss at 270°C and 355°C. Thermal decomposition of lignin occurs in the range from 180°C-900°C with undefined maximum mass loss. The minimum mass loss of 2% was observed in the temperature range from 400°C-900°C. This is referred to as the char formation zone of thermal decomposition, indicating the presence of fixed carbon and non-combustion products (Rout et al. 2016). From the TGA and DTG results, it was found that 200°C-600°C is the suitable temperature for the pyrolysis zone.

Table 3: Percentage of localized carbon, oxygen, and some minerals contents.

S.No.	Element	Weight [%]	Atomic [%]
1	Carbon (C)	76.74	83.87
2	Oxygen (O)	16.80	13.78
3	Magnesium (Mg)	0.65	0.35
4	Silicon (Si)	0.86	0.40
5	Chloride (Cl)	0.37	0.14
6	Potassium (K)	1.54	0.52
7	Calcium (Ca)	2.71	0.89
8	Bromide (Br)	0.33	0.05

FTIR Analysis

FTIR is informative in the determination of various functional groups on the surface of material produced at different conditions**.** The FTIR spectrum of *C. burhia* biochar represented in Fig. 6 shows a very weak banding at

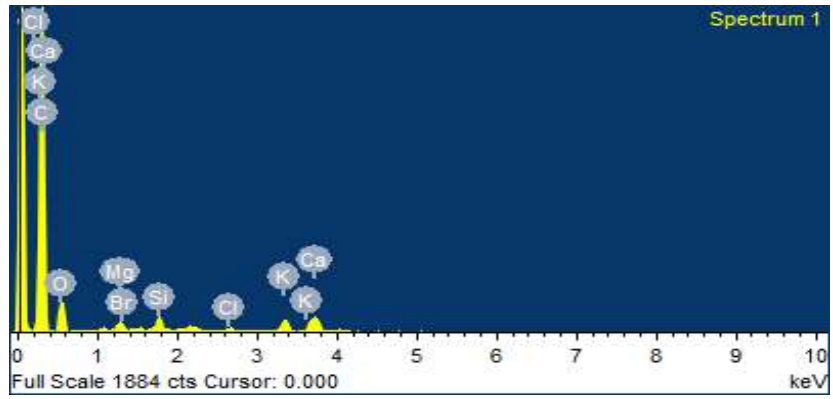

Fig. 4: EDX curves of biochars.

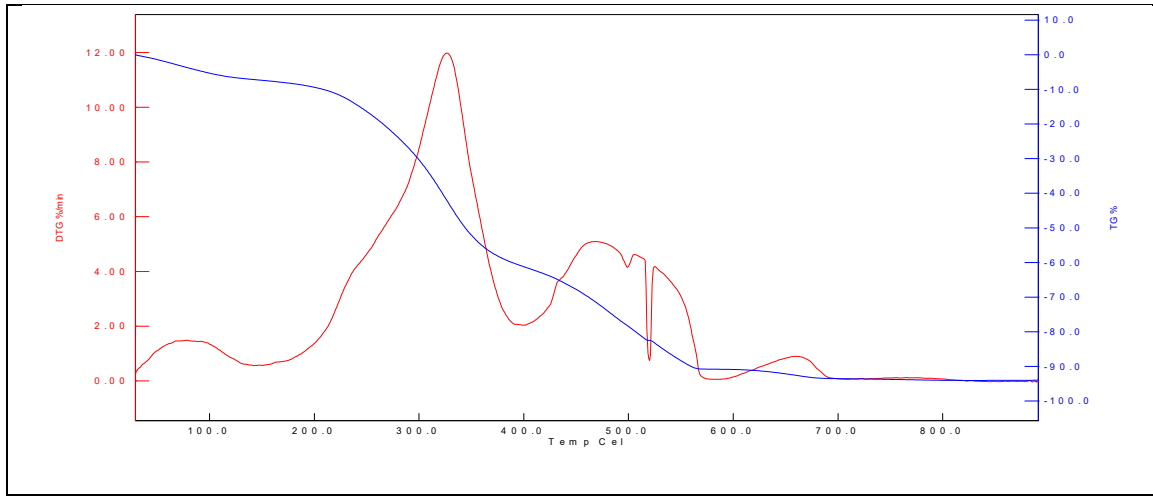

Fig. 5: TG (Thermogravematric) and DTG (derived thermogravematric) curve of *C. burhia*.

2877 cm^{-1}, which represents symmetrical –CH stretching of the aliphatic alkane group. This is similar to a study by Ferreira et al. (2013), who found that major peaks at 2920 cm^{-1} and 2851 cm^{-1} are mainly attributed to the aliphatic chains of suberin, accounting for asymmetric and symmetric -CH stretching vibrations, respectively. Clear peaks representing hemicellulose and cellulose (3200 cm^{-1} -3000 cm^{-1} for OH or 3100 cm^{-1} -3000 cm^{-1} for CH) show degradation of hemicellulose and cellulose at given pyrolytic temperature (Jouiad et al. 2015). Bending at 2340 cm^{-1} indicates the presence of CO_2 (Schott et al. 2021). Between 2000 cm^{-1}-1500 cm^{-1}, two peaks are observed at 1798 cm^{-1} and 1561 cm^{-1}. The absorption band at 1798 cm^{-1} represents the C=O stretching of aldehydes and ketones formed due to the degradation of hemicellulose and cellulose, and the peak at 1561 cm^{-1} denotes plane C=C aromatic vibrations of skeletal compounds in lignin and its extractives (Azargohar et al. 2014, Jouiad et al. 2015). Peaks between a range of 1400 cm^{-1} -900 cm^{-1} represent C=C rings of lignin. Emergences of peaks at 1375 cm^{-1} and 1021 cm^{-1} could be attributed to symmetrical and asymmetrical aryl alkyl ethers showing changes in vibration due to the transformation products of cellulose and lignin components of the biomass. These peaks are more pronounced than those for cellulose and hemicellulose, which can be attributed to lignin degradation temperature between 200°C -and 700°C (Cantrell et al. 2012, Azargohar et al. 2014, Jouiad et al. 2015). Between 900 cm^{-1} -700 $cm^{-1,}$ peaks are observed at 872 cm^{-1}, 808 $cm^{-1,}$ and 745 cm^{-1}, representing aromatic C-H bending vibration of benzene rings (Xu et al. 2013). The presence of various functional groups, such as hydroxyl, aldehyde, and ketone, provides surface binding of polar contaminants (Inyang et al. 2016). Biochar rich in oxygen contains functional groups such as ether that can be considered for the adsorption of heavy metals like cadmium by ion exchange and surface complexation (Fan et al. 2018). FTIR results

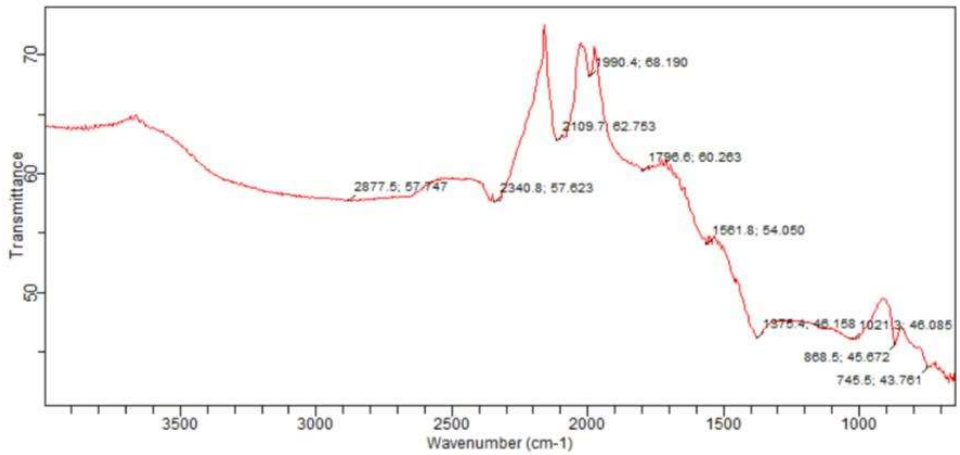

Fig. 6: Spectral bands of FTIR of *C. burhia* biochar.

show that due to pyrolysis at 450°C there occurs degradation of cellulose, hemicellulose, and lignin, but some aromatics related to lignin remained in the biochar.

Statistical Significance of RSM Results of *C. burhia*

Table 4 shows the ANOVA results for responses to fixed carbon, carbon, surface area, pore volume, and pore size, respectively, based on the RSM study employed by the design expert 13.0 software. The model F-value for responses fixed carbon, carbon, surface area, pore volume, and pore size were found as 69.90, 113.40, 1238.31, 21.21, and 19.16, respectively, implying the model is significant, and there is only a 0.01%, 0.01%, 0.01%, 0.04%, and 0.06% respectively chance that an F-value this large could occur due to noise. In this case, A, B, AB, and AB2 are significant model terms (A: temperature, B: particle size). For all the responses, P-values reported less than 0.0500 indicate model terms are significant. Thus, the hypothesis of the present study that particle size and temperature possess a significant effect on all the selected responses is confirmed.

Further, statistical fitting analysis of fixed carbon, carbon, surface area, pore size, and pore volume reveal R^2 values of 0.9804, 0.9878, 0.9989, 0.9381, and 0.9319 which represent significant values (close to 1.00) for the regression model. For fixed carbon, the predicted R^2 of 0.8126 is in reasonable agreement with the adjusted R^2 of 0.9663, with a difference of less than 0.2, which shows the model can predict the response accurately. Similar results were observed for carbon, surface area, and pore size where predicted R^2 (0.8764, 0.9934, and 0.7102, respectively) was found with reasonable agreement with the adjusted R^2 (0.9791, 0.9981, and 0.8833, respectively) and difference less than 2, thus model is excellent to predict the response accurately. Fit statistics for pore volume show that the predicted R^2 of 0.6175 is not as close to the adjusted R^2 of 0.8938 with a difference of more than 0.2. This may indicate a large block effect or a possible problem with the used model and/or data. Adeq Precision measures the signal-to-noise ratio. Adeq precision value of fixed carbon, carbon, surface area, pore volume, and pore size are found to be 25.488, 33.924, 110.126, 16.47, and 14.098, respectively, offering an adequate signal-to-noise ratio as these are higher than 4 (desirable value). This model can be used to navigate the design space. The coefficient of variation (CV %) for all the responses is observed to be less than 10%, representing a good model (Table 5).

Fig. 7(a) (b) (c) (d) (e) shows the correlation between the predicted and actual plot, and linearity shows that the employed model is useful for predicting the fixed carbon, carbon, surface area, pore volume, and pore size efficiently. The predicted value was found to be closely packed around the regression line. Thus predicted and actual values to get good quality biochar are in good agreement. Hence employed model has accurately produced the experimental results. Figs. 8 and 9 display the three-dimensional RSM plots and contour plots of the various components. From the quadratic regression model of ANOVA for various responses of *C. burhia* biochar, the response surface three-dimensional plots (steep slope) and contour plots ie. Two-dimensional plots (elliptical shape) were obtained, representing the significant interaction of particle size and temperature with fixed carbon, carbon, surface area, pore size, and pore volume (Figs. 8 and 9). Plots show the attractiveness at particle sizes ranging between 50 and 100 mm, according to Fig. 8a. The reactivity area decreases with increasing particle size, which may be related to increased pyrolysis and higher ash conversion. The optimization overlay plot (Fig. 10) indicates the optimum conditions of good quality biochar preparation in relation to the fixed carbon, carbon, surface area, pore size,

Table 4: ANOVA for quadratic model based on RSM design for various responses of *C. burhia*.

Response	Source	Sum of Squares	Df	Mean Square	F-value	p-value	
Fixed carbon	Model	0.1187	5	0.0237	69.90	< 0.0001	Significant
	A-Temperature	0.0622	1	0.0622	183.15	< 0.0001	
	B-Particle size	0.0065	1	0.0065	19.07	0.0033	
	AB	0.0028	1	0.0028	8.26	0.0239	
	A^2	0.0432	1	0.0432	127.27	< 0.0001	
	B^2	0.0004	1	0.0004	1.27	0.2967	
Carbon	Model	0.1445	5	0.0289	113.40	< 0.0001	Significant
	A-Temperature	0.0921	1	0.0921	361.34	< 0.0001	
	B-Particle size	0.0151	1	0.0151	59.19	0.0001	
	AB	0.0053	1	0.0053	20.79	0.0026	
	A^2	0.0318	1	0.0318	124.92	< 0.0001	
	B^2	0.0030	1	0.0030	11.86	0.0108	
Surface area	Model	0.0058	5	0.0012	1238.31	< 0.0001	Significant
	A-Temperature	0.0015	1	0.0015	1596.29	< 0.0001	
	B-Particle size	0.0009	1	0.0009	937.94	< 0.0001	
	AB	1.435E-06	1	1.435E-06	1.52	0.2568	
	A^2	0.0028	1	0.0028	2986.13	< 0.0001	
	B^2	9.100E-06	1	9.100E-06	9.67	0.0171	
Pore volume	Model	0.0000	5	2.165E-06	21.21	0.0004	Significant
	A-Temperature	1.299E-06	1	1.299E-06	12.72	0.0091	
	B-Particle size	5.168E-06	1	5.168E-06	50.61	0.0002	
	AB	1.489E-07	1	1.489E-07	1.46	0.2664	
	A^2	3.109E-06	1	3.109E-06	30.45	0.0009	
	B^2	8.928E-08	1	8.928E-08	0.8744	0.3809	
Pore Size	Model	0.0003	5	0.0001	19.16	0.0006	Significant
	A-Temperature	0.0000	1	0.0000	7.59	0.0283	
	B-Particle size	0.0001	1	0.0001	18.71	0.0035	
	AB	7.635E-07	1	7.635E-07	0.2353	0.6424	
	A^2	0.0002	1	0.0002	60.47	0.0001	
	B^2	1.547E-07	1	1.547E-07	0.0477	0.8334	

Table 5: Fit statistics of fixed carbon, carbon, surface area, pore volume and pore size

Responses	Std. Dev.	Mean	C.V.%	R^2	Adjusted R^2	Predicted R^2	Adeq Precision
Fixed carbon	0.0184	8.95	0.2060	0.9804	0.9663	0.8126	25.4881
Carbon	0.0160	9.21	0.1734	0.9878	0.9791	0.8764	33.9242
Surface area	0.0010	9.97	0.0097	0.9989	0.9981	0.9934	110.1255
Pore Volume	0.0003	0.1980	0.1614	0.9381	0.8938	0.6175	16.4706
Pore size	0.0018	2.89	0.0624	0.9319	0.8833	0.7102	14.0979

and pore volume. At ideal temperatures, the bigger surface area and pore volume are desirable for effective adsorption. At 450°C, three distinct *C. burhia* particle sizes were examined. From the overlay optimization plot of the RSM model, it is deducted that maximum fixed carbon, carbon, surface area, pore volume, and pore size may be found at 462.930°C, which is in good agreement with the outcomes at 450°C.

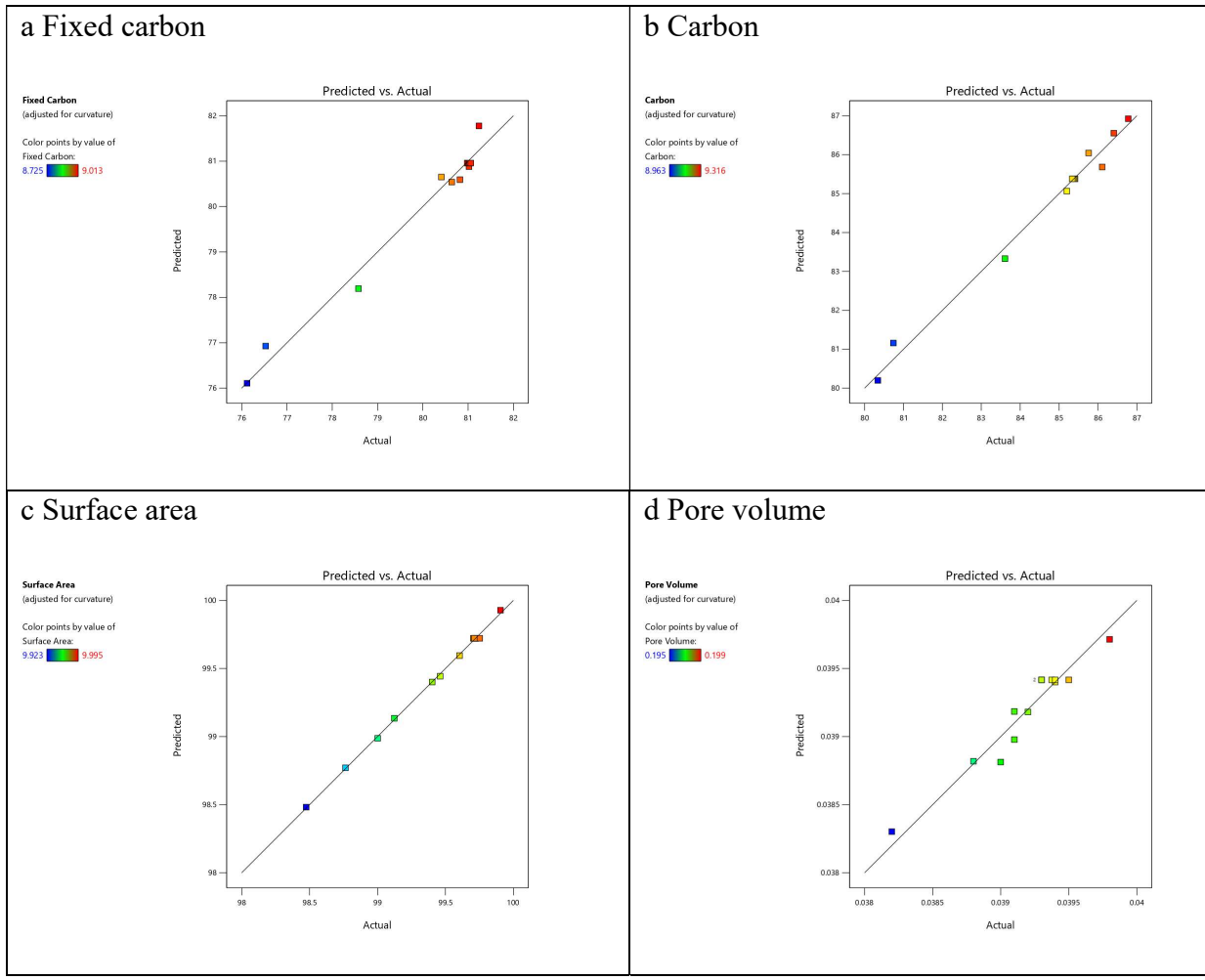

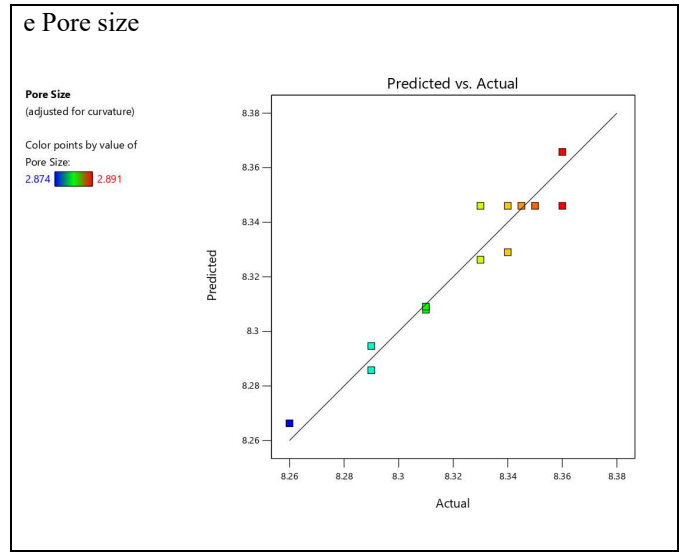

Fig. 7: Predicted vs. actual plots of responses for *C. burhia*.

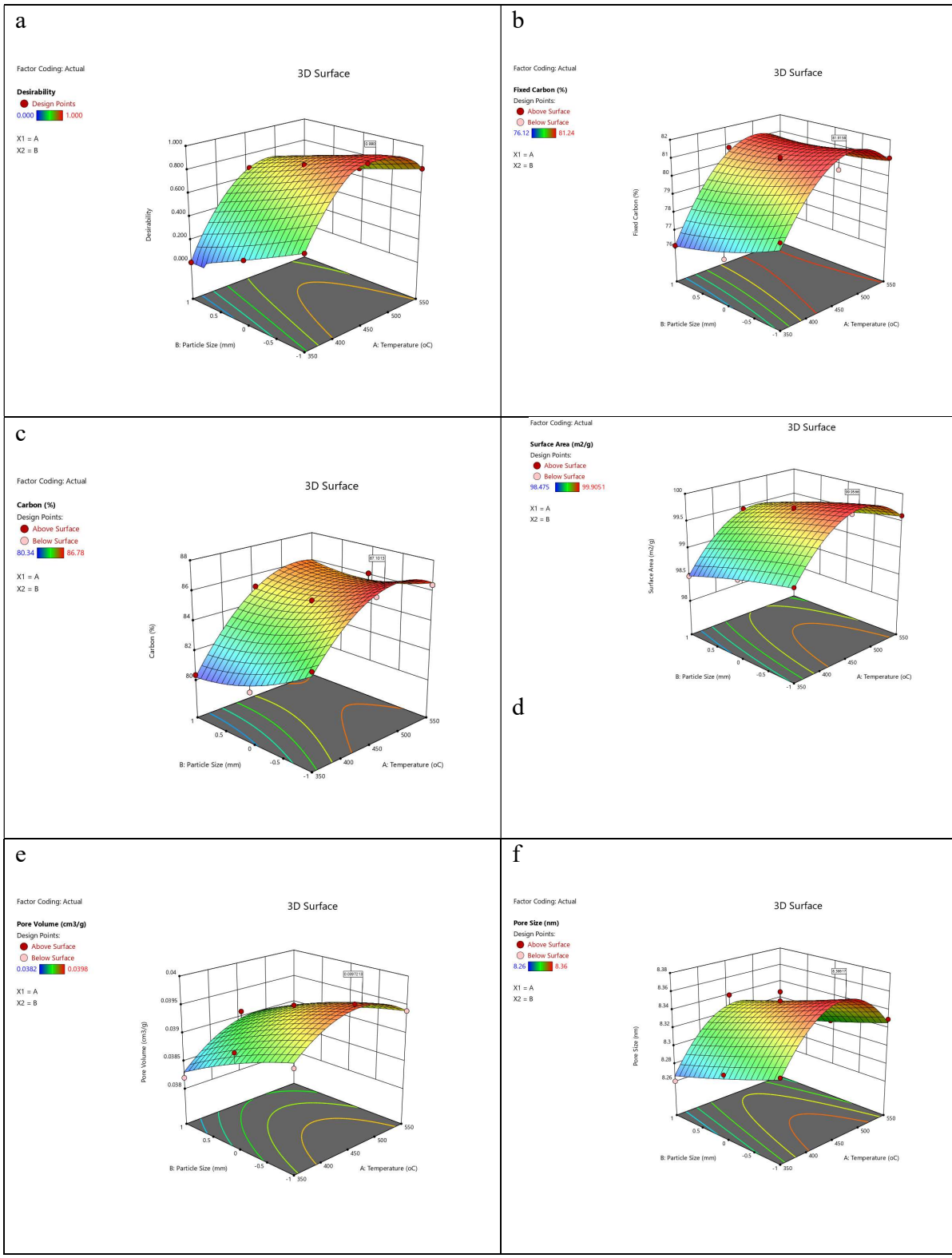

Fig. 8: Three-dimensional response surface plots for desirability, fixed carbon, carbon, surface area, pore volume, and pore size of *C. burhia*.

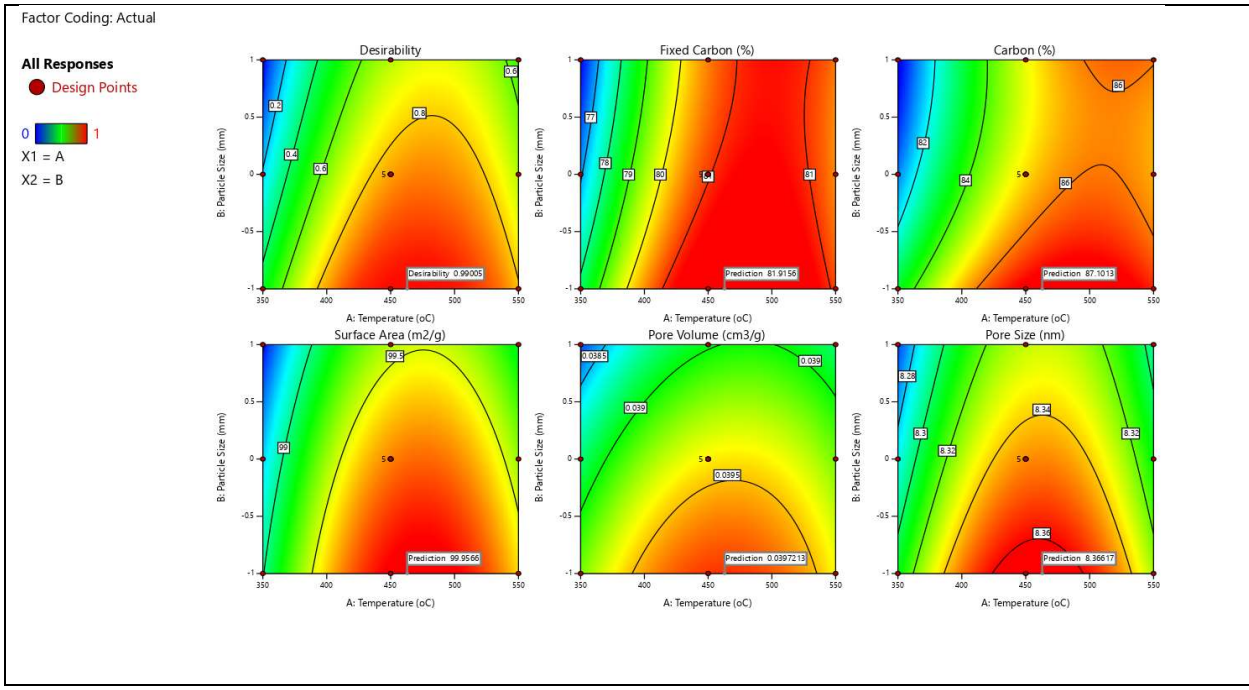

Fig. 9: Contour plots of different responses with particle size and temperature of *C. burhia*.

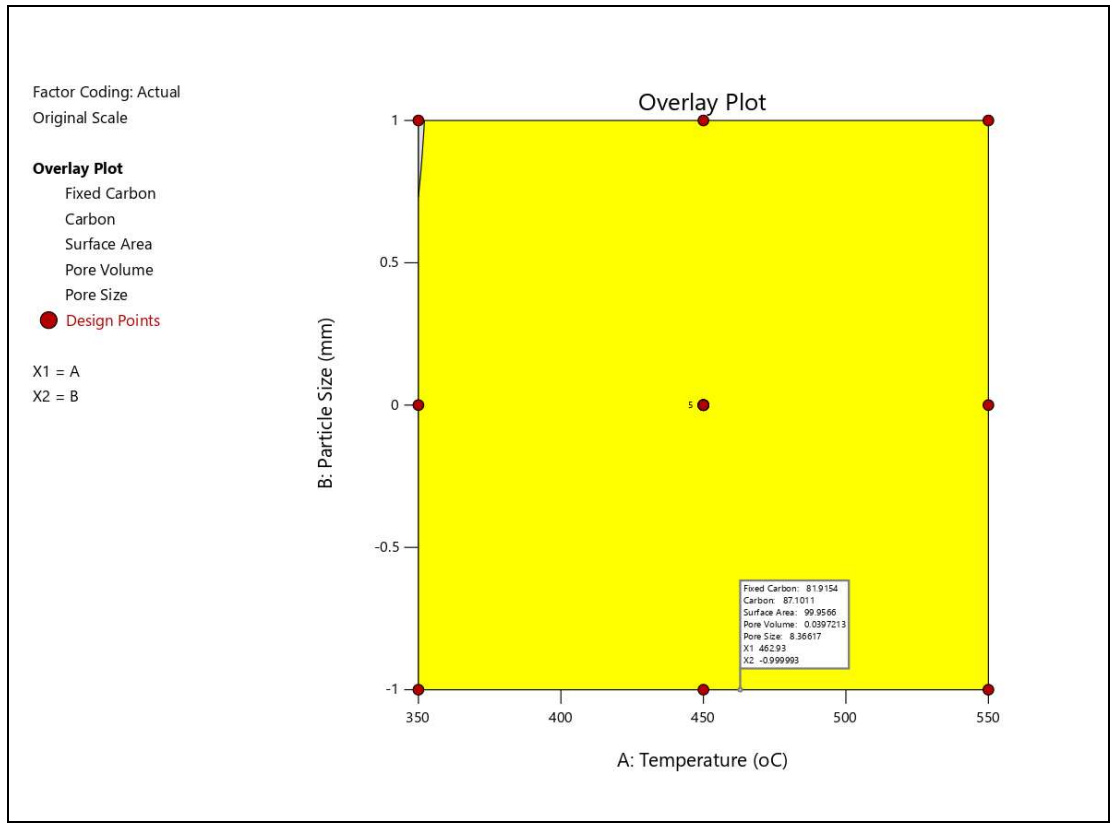

Fig. 10: Overlay plot of *C. burhia*.

CONCLUSIONS

The invasive weed plant feedstock as a resource for biochar production not only reduces the negative environmental impact but also contributes as a bioenergy source for ecological and economic profits. The findings of this study demonstrate that the invasive weed *C. burhia* is a potential source of raw material for biochar production due to its huge biomass, rapid growth, and easy availability. The present study utilized response surface methodology using CCD for the optimization of preparation conditions to obtain good quality biochar. RSM displayed that pyrolytic temperature and feedstock particle size greatly influence the biochar quality parameters such as fixed carbon, carbon, surface area, pore volume, and pore size. The pyrolytic temperature of 450^{o}C (predicted value-462.90^{o}C) and particle size of 50-100mm have been observed for maximum fixed carbon, carbon, surface area, pore volume, and pore size. The slow pyrolysis, along with vacuum conditions, has proven its potential for the production of good quality biochar with high yield, increased surface area, and enhanced fixed carbon content. A low molar ratio of H/C and O/C indicates that biochar is highly carbonized and hydrophobic in nature. SEM/EDX analysis confirms its porous structure with the presence of meso-pores along with some inorganic elements such as calcium, silicon, magnesium, etc. FTIR analysis reports its richness in hydroxyl and carboxyl functional groups. It is expected that obtained biochar is multifunctional and can contribute to climate mitigation, increase carbon sequestrations, enhance soil fertility, and remediation of organic and inorganic pollutants from soil and water.

ACKNOWLEDGEMENTS

The authors are very grateful to Dr. N.L. Panwar Head of Department, Renewable Energy Engineering, Maharana Pratap University of Agriculture and Technology (MPUAT), Udaipur, Rajasthan, India for their support and guidance to drive towards quality research and providing necessary laboratory facilities.

REFERENCES

Azargohar, R., Nanda, S., Kozinski, J., Dalai, A. and Sutarto, R., 2014. Effects of temperature on the physicochemical characteristics of fast pyrolysis bio-chars derived from Canadian waste biomass. *Fuel*, 125, pp.90-100. http://doi.org/10.1016/j.fuel.2014.01.083

Bridgwater, A.V., 2003. Renewable fuels and chemicals by thermal processing of biomass. *Journal of Chemical Technology & Biotechnology*, 91(2-3), pp.87-102

Cantrell, B., Hunt, P.G., Uchimiya, M., Novak, J.M. and Ro, K.S., 2012. Impact of pyrolysis temperature and manure source on physic-chemical characteristics of biochar. *Bioresource Technology*, 107, pp.419-428.

Carrier, M., Hardie, A.G., Uras, Ü., Görgens, J. and Knoetze, J., 2012. Production of char from vacuum pyrolysis of South African sugar cane bagasse and its characterization as activated carbon and biochar. *Journal of Analytical and Applied Pyrolysis*, 96, pp.24–32. https://doi.org/10.1016/j.jaap.2012.02.016

Cheah, S., Jablonski, W.S., Olstad, J.L., Carpenter, D.L., Barthelemy, K.D., Robichaud, D.J., Andrews, J.C., Black, S.K., Oddo, M.D. and Westover, T.L., 2016. Effects of thermal pretreatment and catalyst on biomass gasification efficiency and syngas composition. *Green Chemistry*, 18, pp.6291–6304

Chen, B., Zhou, D. and Zhu, L., 2008. Transitional adsorption and partition of nonpolar and polar aromatic contaminants by biochars of pine needles with different pyrolytic temperatures. *Environmental Science & Technology*, 42, pp.5137-5143

Chen, X., Chen, G., Chen, L., Chen, Y., Lehmann, J., McBride, M.B. and Hay, A.G., 2011. Adsorption of copper and zinc by biochars produced from pyrolysis of hardwood and corn straw in aqueous solution. *Bioresource Technology*, 102(19), pp.8877-8884

Daful, A.G., Chandraratne, M.R. and Loridon, M., 2021. Recent perspectives in biochar production, characterization and applications. In: Bartoli, M. and Giorcelli, M. (eds.) *Recent Perspectives in Pyrolysis Research*. IntechOpen, pp. 327-344.

Daful, A.G. and Chandraratne, M.R., 2020. Biochar production from biomass waste-derived material. In: Hashmi, S., Choudhury, I.A. (eds.). *Encyclopedia of Renewable and Sustainable Materials*. Oxford: Elsevier; pp. 370-378.

De la Rosa, J.M., Paneque, M., Miller, A.Z. and Knicker, H., 2014. Relating physical and chemical properties of four different biochars and their application rates to biomass production of *Lolium perenne* on a Calcic Cambisol during a pot experiment of 79 days. *Science of The Total Environment*, 499, pp.175-184.

Domingues, R.R., Trugilho, P.F., Silva, C.A., de Melo, I.C.N.A., Melo, L.C.A., Magriotis, Z.M. and Sánchez-Monedero, M.A., 2017. Properties of biochar derived from wood and high-nutrient biomasses with the aim of agronomic and environmental benefits. *PLoS ONE*, 12, e0176884.

Fan, S.S., Wang, Y., Li, Y., Wang, Z., Xie, Z.X. and Tang, J., 2018. Removal of tetracycline from aqueous solution by biochar derived from rice straw. *Environmental Science and Pollution Research*, 25(29), pp.29529–29540.

Feng, Q., Wang, B., Chen, M., Wu, P., Lee, X. and Xing, Y., 2021. Invasive plants as potential sustainable feedstocks for biochar production and multiple applications: A review. *Resources, Conservation and Recycling*, 164, 105204.

Ferreira, R., Garcia, H., Sousa, A.F., Freire, C.S.R., Silvestre, A.J.D., Rebelo, L.P.N. and Pereira, C.S., 2013. Isolation of suberin from birch outer bark and cork using ionic liquids: a new source of macromonomers. *Industrial Crops and Products*, 44, pp.520–527. https://doi.org/10.1016/j.indcrop.2012.10.002

IBI, 2015. Standardized product definition and product testing guidelines for biochar that is used in soil. *International Biochar Initiative*, Version 2.1.

Inyang, M.I., Gao, B., Yao, Y., Xue, Y., Zimmerman, A., Mosa, A., Pullammanappallil, P., Ok, Y.S. and Cao, X., 2016. A review of biochar as a low-cost adsorbent for aqueous heavy metal removal. *Critical Reviews in Environmental Science and Technology*, 46, pp.406-433.

Jha, P., Neenu, S., Rashmi, I., Meena, B.P., Jatav, R.C., Lakaria, B.L., Biswas, A.K., Singh, M. and Patra, A.K., 2010. Ameliorating effects of Leucaena biochar on soil acidity and exchangeable ions. *Communications in Soil Science and Plant Analysis*, 47(10), pp.1252-1262.

Jouiad, M., Al-Nofeli, N., Khalifa, N., Benyettou, F. and Yousef, L.F., 2015. Characteristics of slow pyrolysis biochars produced from Rhodes grass and fronds of edible date palm. *Journal of Analytical and Applied Pyrolysis*, 111, pp.183.

Kambo, H. and Dutta, A., 2015. A comparative review of biochar and hydrochar in terms of production, physico-chemical properties, and applications. *Renewable and Sustainable Energy Reviews*, 45, pp.359–378. http://doi.org/10.1016/j.rser.2015.01.050

Kan, T., Strezov, V. and Evans, T.J., 2016. Lignocellulosic biomass pyrolysis: A review of product properties and effects of pyrolysis parameters. *Renewable and Sustainable Energy Reviews*, 57(C), pp.1126-1140.

Kumar, S., Praveen, F., Goyal, S. and Chauhan, A., 2008. Indigenous herbal coolants for combating heat stress in the hot Indian Arid Zone. *Indian Journal of Traditional Knowledge*, 7(4), pp.679-682.

Lehmann, J. and Joseph, S., 2009. *Biochar for Environmental Management: Science and Technology*. Earthscan.

Lewis, G.P., 2005. *Legumes of the World*. Royal Botanic Gardens Kew.

Li, X., Shen, Q., Zhang, D., Mei, X., Ran, W., Xu, Y., Yu, G. and Motta, A., 2013. Functional groups determine biochar properties (pH and EC) as studied by two-dimensional 13C NMR correlation spectroscopy. *PLoS ONE*, 8(6), e65949.

Masto, L.E., Kumar, S., Rout, T.K., Sarkar, P., George, J. and Ram, L.C., 2013. Biochar from water hyacinth (*Eicchornia crassipes*) and its impact on biological activity. *CATENA*, 111, pp.64-71.

Park, J., Lee, Y., Ryu, C. and Park, Y.K., 2014. Slow pyrolysis of rice straw: Analysis of product properties, carbon and energy yields. *Bioresource Technology*, 155, pp.63-70. https://doi.org/10.1016/j.biortech.2013.12.084

Parshetti, G.K., Hoekman, S.K. and Balasubramanian, R., 2013. Chemical, structural, and combustion characteristics of carbonaceous products obtained by hydrothermal carbonization of palm empty fruit bunches. *Bioresource Technology*, 135, pp.683–689.

Pawar, A. and Panwar, N.L., 2022. A comparative study on morphology, composition, kinetics, thermal behavior, and thermodynamic parameters of *Prosopis juliflora* and its biochar derived from vacuum pyrolysis. *Bioresource Technology Reports*, 18, 101053.

Premjet, S., 2018. *Potential of Weed Biomass for Bioethanol Production in Fuel Ethanol Production from Sugarcane*. Intech Open, pp.83–98.

Priya, H.R., Veena, A.H., Pavithra, D. and Joythi, A., 2014. Prospects and problems of utilization of weed biomass: A review. *Research & Reviews: Journal of Agricultural and Allied Sciences*, 3, pp.1–11.

Qian, K., Kumar, A., Patil, K., Bellmer, D., Wang, D., Yuan, W. and Huhnke, R., 2013. Effects of biomass feedstocks and gasification conditions on the physiochemical properties of char. *Energies*, 6(8), pp.3972-3986. http://doi.org/10.3390/en6083972

Rafiq, M.K., Bachmann, R.T., Rafiq, M.T., Shang, Z., Joseph, S. and Long, R., 2016. Influence of pyrolysis temperature on physico-chemical properties of corn stover (*Zea mays* L) biochar and feasibility for carbon capture and energy balance. *PLoS ONE*, 11, e0156894.

Rivka, B., Laird, D., Thompson, M. and Lawrinenko, M., 2017. Characterization and quantification of biochar alkalinity. *Chemosphere*, 167, pp.367-373. http://doi.org/10.1016/j.chemosphere.2016.09.151

Rodriguez, J.A., Lustosa, J.F., Melo, L.C.A., de Assis, I.R. and de Oliveira, T.S., 2020. Influence of pyrolysis temperature and feedstock on the properties of biochars produced from agricultural and industrial wastes. *Journal of Analytical and Applied Pyrolysis*, 149, 104839.

Ronsse, F., Dickinson, D., Nachenius, R. and Prins, W., 2013. Biomass pyrolysis and biochar characterization. In *Proceedings of the 1st FOREBIOM Workshop*, 4(4).

Rout, T., Pradhan, D., Singh, R.K. and Kumari, N., 2016. An exhaustive study of products obtained from coconut shell pyrolysis. *Journal of Environmental Chemical Engineering*, 4(3), pp.3696–3705.

Roy, P. and Dias, G., 2017. Prospects for pyrolysis technologies in the bioenergy sector: A review. *Renewable and Sustainable Energy Reviews*, 77, pp.59.

Sadaka, S., Sharara, M.A., Ashworth, A., Keyser, P., Allen, F. and Wright, A., 2014. Characterization of biochar from switchgrass carbonization. *Energies*, 7, pp.548-567.

Salavati-Niasari, M., Davar, F. and Loghman-Estarki, M.R., 2010. Controllable synthesis of thioglycolic acid capped ZnS (Pn)0.5 nanotubes via simple aqueous solution route at low temperatures and conversion to wurtzite ZnS nanorods via thermal decomposition of precursor. *Journal of Alloys and Compounds*, 494(1–2), pp.199–204.

Schott, J.A., Do-Thanh, C.L., Shan, W., Puskar, N.G., Dai, S. and Mahurin, S.M., 2021. FTIR investigation of the interfacial properties and mechanisms of CO_2 sorption in porous ionic liquids. *Green Chemistry*, 2(4), pp.392-401.

Shaaban, A., Se, S.M., Dimin, M.F., Juoi, J.M., Husin, M.H. and Mitan, N.M., 2014. Influence of heating temperature and holding time on biochars derived from rubber wood sawdust via slow pyrolysis. *Journal of Analytical and Applied Pyrolysis*, 107, pp.31–39.

Sik, Y., Uchimiya, S., Chang, S. and Bolan, N., 2016. *Biochar: Production, Characterization and Applications*. CRC Press.

Song, W. and Guo, M., 2012. Effect of pyrolysis temperature and feedstock type on agricultural properties and stability of biochars. *Journal of Analytical and Applied Pyrolysis*, 94, p.138.

Spokas, K., 2010. Review of the stability of biochar in soils: Predictability of Omolar ratios. *Carbon Management*, 1(2). https://doi.org/10.4155/cmt.10.32

Tomczyk, A., Sokołowska, Z. and Boguta, P., 2020. Biochar physicochemical properties: Pyrolysis temperature and feedstock kind effects. *Reviews in Environmental Science and Bio/Technology*, 19, pp.191-215.

Tripathi, M., Sahu, J.N. and Ganesan, P., 2016. Effect of process parameters on production of biochar from biomass waste through pyrolysis: A review. *Renewable and Sustainable Energy Reviews*, 55, pp.467.

Uchimiya, M., Ohno, T. and He, Z., 2013. Pyrolysis temperature-dependent release of dissolved organic carbon from plant, manure, and biorefinery wastes. *Journal of Analytical and Applied Pyrolysis*, 104, pp.84-94.

Usman, R., Abduljabbar, A., Vithanage, M., Ok, Y.S., Ahmad, M., Elfaki, J., Abdulazeem, S.S., Al-Wabel, M.I., 2015. Biochar production from date palm waste: Charring temperature-induced changes in composition and surface chemistry. *Journal of Analytical and Applied Pyrolysis*, 115, pp.392.

Wang, L., Olsen, M.N.P., Moni, C., Dieguez-Alonso, A., de la Rosa, M., Stenrød, M., Liu, X. and Mao, I., 2022. Comparison of properties of biochar produced from different types of lignocellulosic biomass by slow pyrolysis at 600 °C. *Applied Energy Combustion Science*, 12, 100090.

Wanjala, C.W. and Majinda, R.T., 1999. Flavonoid glycosides from *Crotalaria podocarpa*. *Phytochemistry*, 51, pp.705-707.

Weber, K. and Quicker, P., 2018. Properties of biochar. *Fuel*, 217, pp.240-261.

Xu, X., Cao, X. and Zhao, L., 2013. Comparison of rice husk-and dairy manure-derived biochars for simultaneously removing heavy metals from aqueous solutions: Role of mineral components in biochars. *Chemosphere*, 92(8), pp.955-961.

Yang, H., Yan, R., Chen, H., Lee, D.H. and Zheng, C., 2007. Characteristics of hemicellulose, cellulose, and lignin pyrolysis. *Fuel*, 86, pp.1781-1788.

Yuan, J.H., Xu, R.K. and Zhang, H., 2011. The forms of alkali in biochar produced from crop residues at different temperatures. *Bioresource Technology*, 102, pp.3488-3497.

Zama, E.F., Zhu, Y.G., Reid, B.J. and Sun, G.X., 2017. The role of biochar properties in influencing the sorption and desorption of Pb (II), Cd

(II), and As (III) in aqueous solution. *Journal of Cleaner Production*, 148, pp.127-136.

Zhang, J. and Liy, R., 2015. Effects of pyrolysis temperature and heating time on biochar obtained from pyrolysis of straw and lignosulphonate. *Bioresource Technology*, 176, pp.288-291.

Zhao, S.X., Na, T. and Wang, X.D., 2017. Effect of temperature on the structural and physicochemical properties of biochar with apple tree branches as feedstock material. *Energies*, 10, 1293.

ORCID DETAILS OF THE AUTHORS

Loveena Gaur: https://orcid.org/0009-0008-4613-3905
Poonam Poonia: https://orcid.org/0000-0002-7766-1830